Supplementary Information for

Unraveling Interphase-Driven Failure Pathways in $LiMn_{0.6}Fe_{0.4}PO_4$/Graphite Pouch Cells

Chanmonirath (Michael) Chak[a], Vadim Shipitsyn[a], Ruiyi Song[b], Glenn Pastel[c]*, Wenhua Zuo[d], Yuwei Zhu[e], Gui-Liang Xu[d], Linqin Mu[e], Lin Ma[a]*

a. Department of Applied Physical Sciences, University of North Carolina at Chapel Hill, Chapel Hill, NC 27514, USA
b. DP Technology, Delaware, USA
c. Battery Sciences Branch, DEVCOM Army Research Laboratory, Adelphi, MD 20783, USA
d. Chemical Sciences and Engineering Division, Argonne National Laboratory, Lemont, IL 60439 USA
e. Materials Science Engineering, School of Engineering for Matter, Transport, and Energy, Arizona State University, Tempe, AZ 85281, USA

E-mail: glenn.r.pastel.civ@army.mil; l.ma@unc.edu

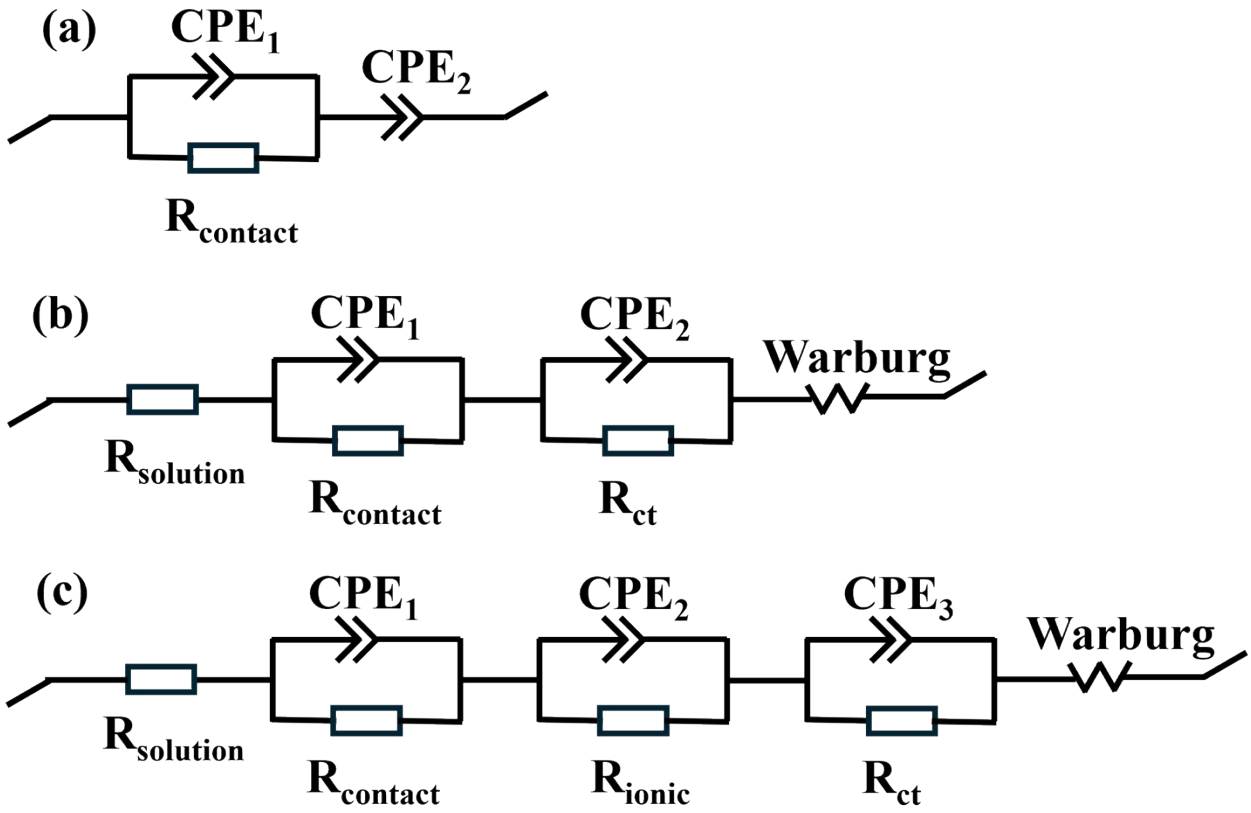

Figure S1. Equivalent circuit models used for fitting for (a) the contact resistance[1-3] (**Figure S2**), (b) negative symmetric cells[2-5], and (c) positive symmetric cells, full coin cells, and pouch cells[4, 5]. $R_{solution}$ is solution resistance, $R_{contact}$ is contact resistance, R_{ct} is charge transfer resistance, CPE is constant phase element, W is Warburg circuit element.

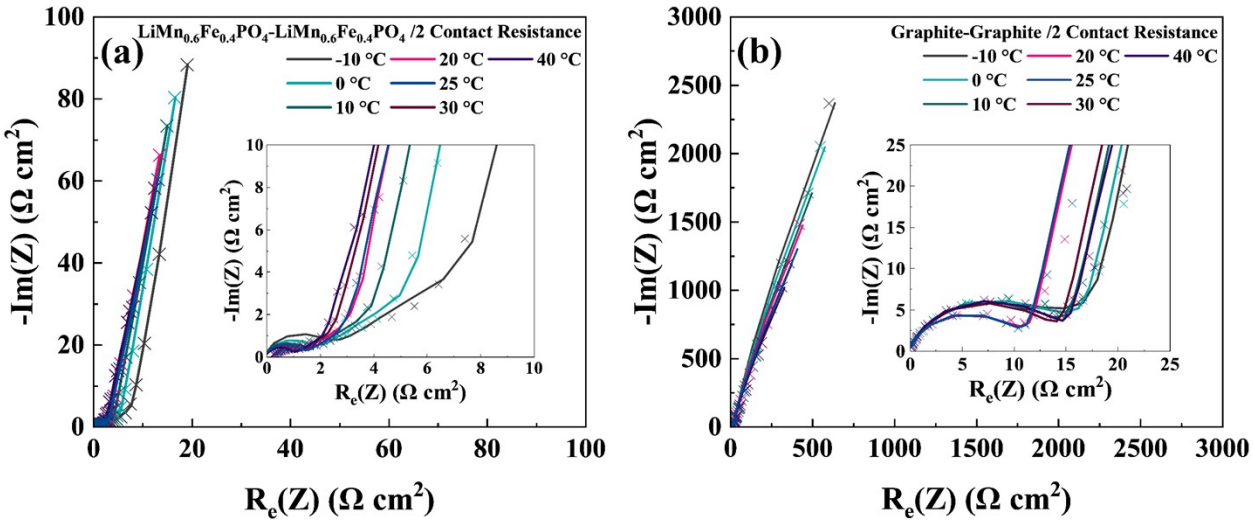

Figure S2. Area specific Nyquist plots of blocking (a) $LiMn_{0.6}Fe_{0.4}PO_4$ cathode ((+/+)/2) and (b) graphite anode ((-/-)/2) symmetric cells at different temperatures. The cells were fabricated using electrodes punched from fresh $LiMn_{0.6}Fe_{0.4}PO_4$/graphite pouch cells. Experimental data are shown as solid line and fitted data are shown as cross symbols, using the equivalent circuit in **Figure S1a**. The average contact resistance ($R_{contact}$) of $LiMn_{0.6}Fe_{0.4}PO_4$ cathode and graphite anode were determined to be 4.53 Ω cm^2 and 14.05 Ω cm^2, respectively.

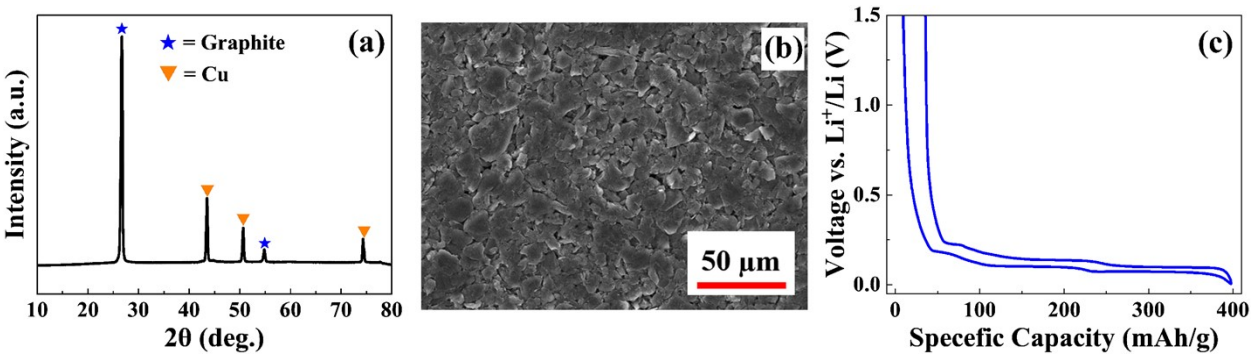

Figure S3. Characterizations of graphite anode material. (a) XRD pattern and (b) SEM image of pristine graphite electrode. (c) Voltage vs. specific capacity curve of graphite/Li half cell cycled at C/20 and 25 ºC.

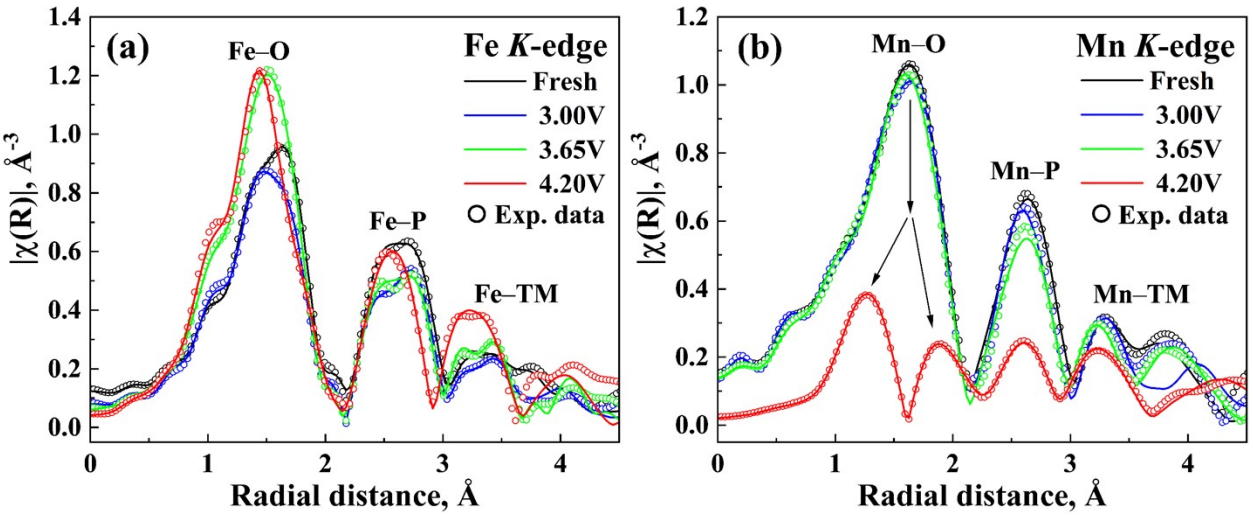

Figure S4. *Ex-situ* EXAFS spectra of (a) Fe K-edge and (b) Mn K-edge in $LiMn_{0.6}Fe_{0.4}PO_4$ electrode at different voltages.

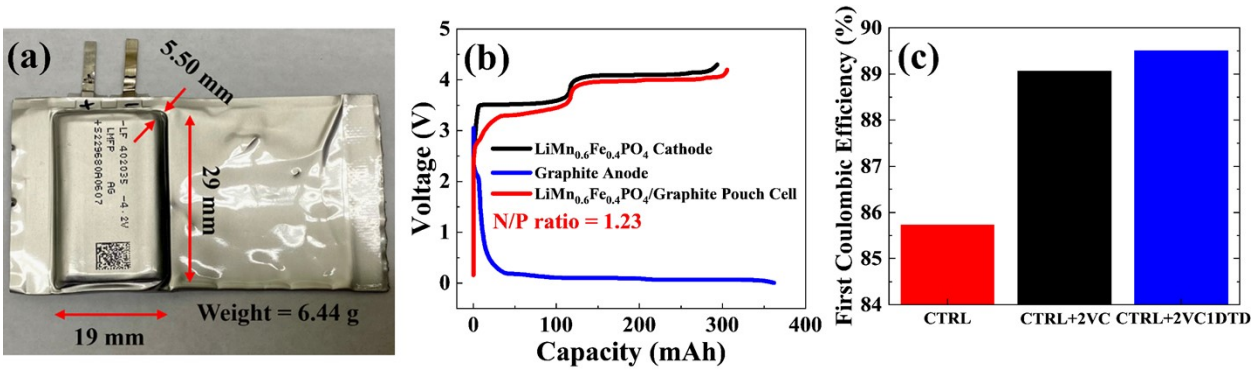

Figure S5. (a) $LiMn_{0.6}Fe_{0.4}PO_4$/graphite pouch cell, (b) voltage vs. capacity curves of $LiMn_{0.6}Fe_{0.4}PO_4$ cathode, graphite anode, and $LiMn_{0.6}Fe_{0.4}PO_4$/graphite pouch cell, displaying N/P ratio of 1.23, (c) first-cycle Coulombic efficiency of $LiMn_{0.6}Fe_{0.4}PO_4$/graphite pouch cells during formation.

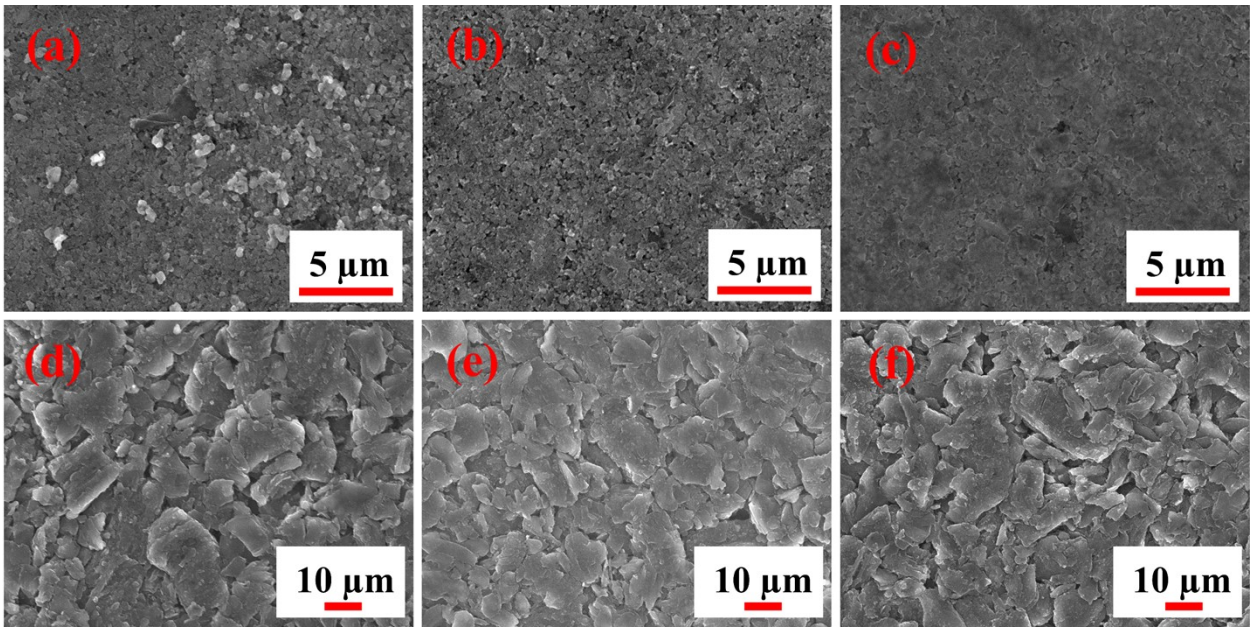

Figure S6. SEM images of (a-c) $LiMn_{0.6}Fe_{0.4}PO_4$ cathode and (d-f) graphite anode after long-term cycling with different electrolytes including (a, d) CTRL, (b, e) CTRL + 2% VC, and (c, f) CTRL + 2% VC + 1% DTD electrolytes.

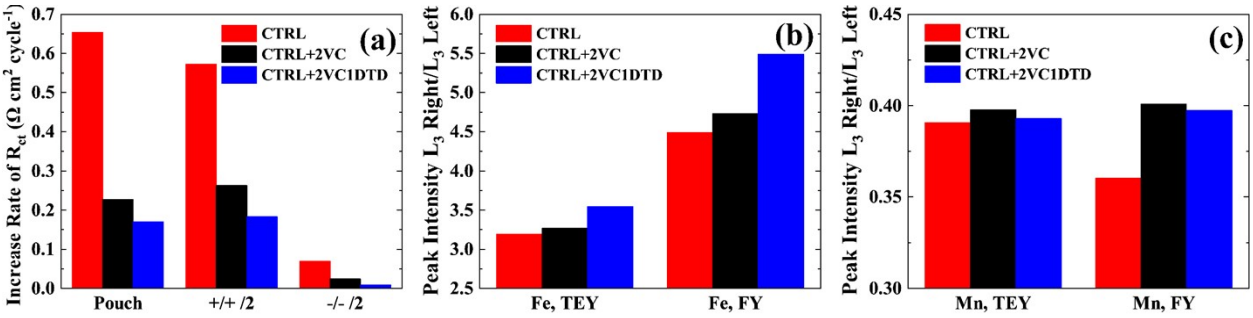

Figure S7. (a) Increase rate of R_{ct} per cycle for $LiMn_{0.6}Fe_{0.4}PO_4$/graphite pouch cell, $LiMn_{0.6}Fe_{0.4}PO_4$ cathode ((+/+)/2) and (b) graphite anode ((-/-)/2) symmetric cells. (b) The Fe L3-edge has two peaks, and the intensity ratio between the right peak and the left peak is plotted as a function of the labeled conditions. (c) The Mn L3-edge has two peaks, and the intensity ratio between the right peak and the left peak is plotted as a function of the labeled conditions.

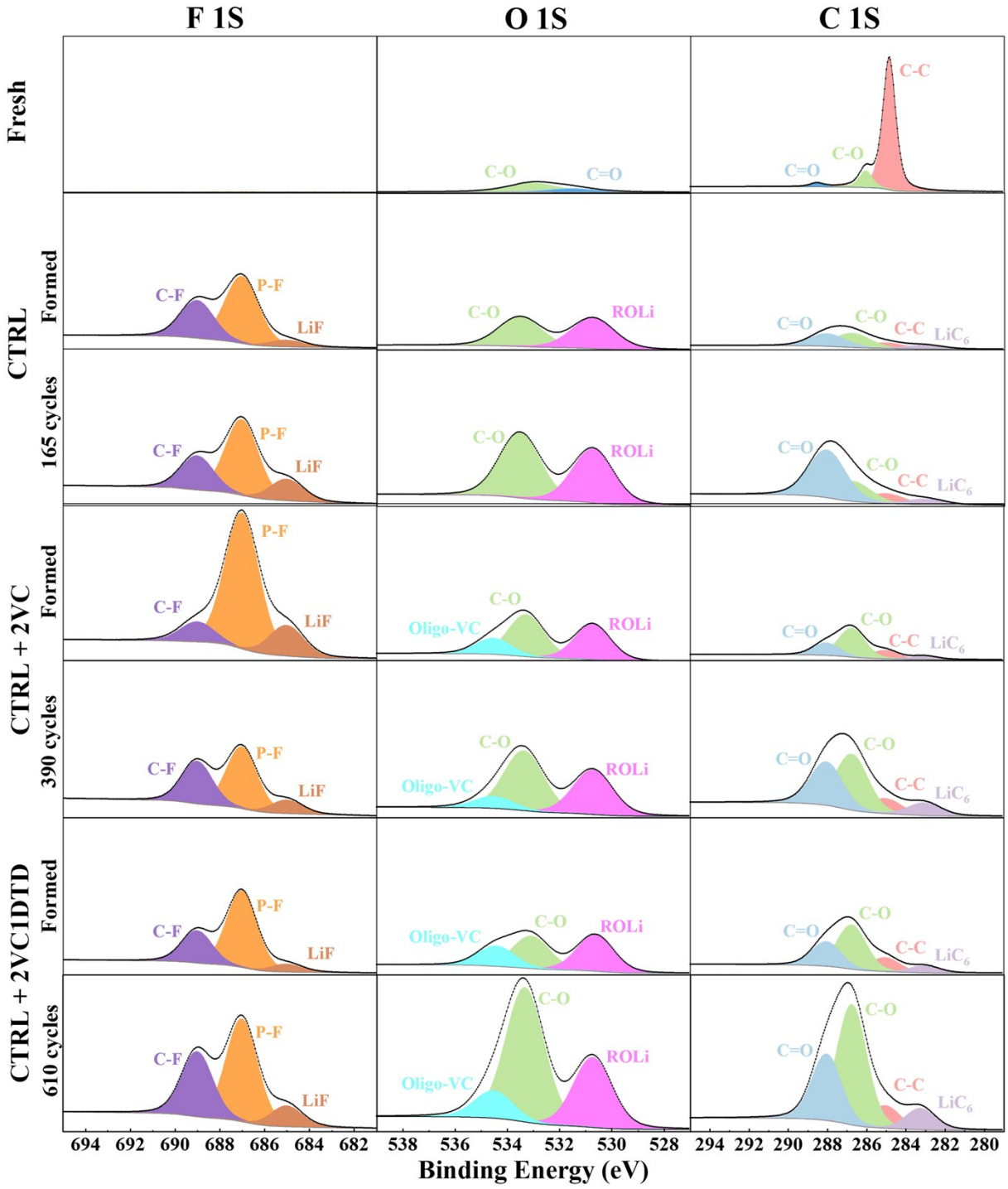

Figure S8. XPS data for graphite electrodes extracted from fresh, formed, and cycled pouch cells. Formed cells were formed to 4.2 V; cycled cells were cycled between 3.0 V and 4.2 V; all formed and cycled cells were disassembled at 3.9 V and contained CTRL, CTRL+2VC, or CTRL+2VC1DTD electrolyte. Each row contains data from one electrode sample. F 1s, O 1s, and C 1s spectra are shown. The y-axis scales are equal for spectra of the same type (columns). Components are labeled based on binding energy and literature assignments (**Table S12**).

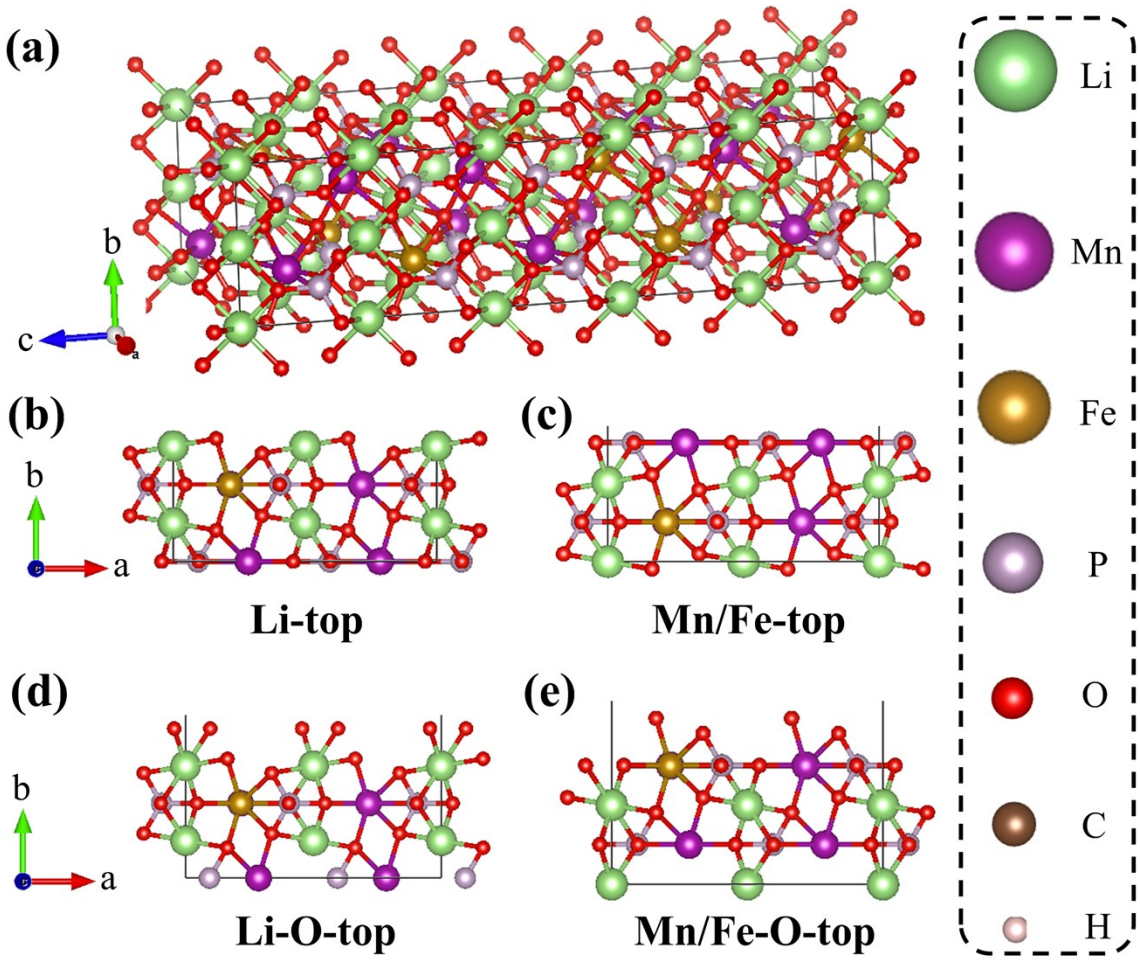

Figure S9. (a) Expanded unit cell of $LiMn_{0.6}Fe_{0.4}PO_4$ to remove partial atom occupations. Four different types of (010) lattice surfaces are shown: (b) Li-top, (c) Mn/Fe-top, (d) Li-O-top, and (e) Mn/Fe-O-top.

Table S1. The best fit parameters for the *ex situ* $LiMn_{0.6}Fe_{0.4}PO_4$ pristine
E_0 = 3.71 +/- 2.93, S_0^2 = 1.053 +/- 0.288, R-factor = 0.0038

Sphere	Bond	N	R, Å	sigma, 10^{-3} Å
1st	Fe-O	2	2.01435	2.53
1st	Fe-O	1	2.11335	1.66
1st	Fe-O	1	2.21067	0.74
2nd	Fe-P	1	2.83298	6.24
2nd	Fe-P	1	3.20688	203.2
2nd	Fe-P	3	3.24557	7.96
3rd	Fe-TM	4	3.83663	26.72
3rd	Fe-TM	2	4.66033	9.65

Table S2. The best fit parameters for the *ex situ* $LiMn_{0.6}Fe_{0.4}PO_4$ 3.00V vs. Li^+/Li
E_0 = 12.42 +/- 3.42, S_0^2 = 1.431 +/- 1.399, R-factor = 0.0029

Sphere	Bond	N	R, Å	sigma, 10^{-3} Å
1st	Fe-O	2	2.00738	7.95
1st	Fe-O	1	2.10730	7.09
1st	Fe-O	1	2.20434	71.27
2nd	Fe-P	1	2.82486	9.41
2nd	Fe-P	1	3.19770	36.12
2nd	Fe-P	3	3.23627	17.61
3rd	Fe-TM	4	3.82564	19.95
3rd	Fe-TM	2	4.64698	15.27

Table S3. The best fit parameters for the *ex situ* $LiMn_{0.6}Fe_{0.4}PO_4$ 3.65V vs. Li^+/Li
E_0 = 4.45 +/- 2.55, S_0^2 = 2.578 +/- 0.829, R-factor = 0.0056

Sphere	Bond	N	R, Å	sigma, 10^{-3} Å
1st	Fe-O	2	2.01126	8.78
1st	Fe-O	1	2.11099	52.46
1st	Fe-O	1	2.20820	232.88
2nd	Fe-P	1	2.82981	15.02
2nd	Fe-P	1	3.20330	19.13
2nd	Fe-P	3	3.24194	24.31
3rd	Fe-TM	4	3.83234	30.45
3rd	Fe-TM	2	4.65512	18.85

Table S4. The best fit parameters for the *ex situ* $LiMn_{0.6}Fe_{0.4}PO_4$ 4.20V vs. Li^+/Li
E_0 = 4.43 +/- 3.28, S_0^2 = 1.754+/- 0.646, R-factor = 0.0175

Sphere	Bond	N	R, Å	sigma, 10^{-3} Å
1st	Fe-O	2	1.93860	4.88
1st	Fe-O	1	2.08908	3.01
1st	Fe-O	1	2.18529	37.39
2nd	Fe-P	1	2.80045	9.60
2nd	Fe-P	1	3.17006	5.39
2nd	Fe-P	3	3.20830	32.20
3rd	Fe-TM	4	3.79257	17.46
3rd	Fe-TM	2	4.60681	14.00

Table S5. The best fit parameters for the *ex situ* $LiMn_{0.6}Fe_{0.4}PO_4$ pristine
E_0 = 3.71 +/- 2.93, S_0^2 = 1.053 +/- 0.288, R-factor = 0.0038

Sphere	Bond	N	R, Å	sigma, 10^{-3} Å
1st	Mn-O	2	2.01435	2.53
1st	Mn-O	1	2.11335	1.66
1st	Mn-O	1	2.21067	0.74
2nd	Mn-P	1	2.83298	6.24
2nd	Mn-P	1	3.20688	203.2
2nd	Mn-P	3	3.24557	7.96
3rd	Mn-TM	4	3.83663	26.72
3rd	Mn-TM	2	4.66033	9.65

Table S6. The best fit parameters for the *ex situ* $LiMn_{0.6}Fe_{0.4}PO_4$ 3.00V vs. Li^+/Li
E_0 = 12.42 +/- 3.42, S_0^2 = 1.431 +/- 1.399, R-factor = 0.0029

Sphere	Bond	N	R, Å	sigma, 10^{-3} Å
1st	Mn-O	2	2.00738	7.95
1st	Mn-O	1	2.10730	7.09
1st	Mn-O	1	2.20434	71.27
2nd	Mn-P	1	2.82486	9.41
2nd	Mn-P	1	3.19770	36.12
2nd	Mn-P	3	3.23627	17.61
3rd	Mn-TM	4	3.82564	19.95
3rd	Mn-TM	2	4.64698	15.27

Table S7. The best fit parameters for the *ex situ* $LiMn_{0.6}Fe_{0.4}PO_4$ 3.65V vs. Li^+/Li
E_0 = 4.45 +/- 2.55, S_0^2 = 2.578 +/- 0.829, R-factor = 0.0056

Sphere	Bond	N	R, Å	sigma, 10^{-3} Å
1st	Mn-O	2	2.01126	8.78
1st	Mn-O	1	2.11099	52.46
1st	Mn-O	1	2.20820	232.88
2nd	Mn-P	1	2.82981	15.02
2nd	Mn-P	1	3.20330	19.13
2nd	Mn-P	3	3.24194	24.31
3rd	Mn-TM	4	3.83234	30.45
3rd	Mn-TM	2	4.65512	18.85

Table S8. The best fit parameters for the *ex situ* $LiMn_{0.6}Fe_{0.4}PO_4$ 4.20V vs. Li^+/Li
E_0 = 8.56 +/- 2.45, S_0^2 = 2.044+/- 0.631, R-factor = 0.0069

Sphere	Bond	N	R, Å	sigma, 10^{-3} Å
1st	Mn-O	2	1.96259	34.80
1st	Mn-O	1	2.14113	83.12
1st	Mn-O	1	2.23973	25.79
2nd	Mn-P	1	2.87022	31.28
2nd	Mn-P	1	3.24904	40.43
2nd	Mn-P	3	3.28824	56.24
3rd	Mn-TM	4	3.88707	39.39
3rd	Mn-TM	2	4.72159	33.64

Table S9. Summary of R_{ct} values for $LiMn_{0.6}Fe_{0.4}PO_4$/$LiMn_{0.6}Fe_{0.4}PO_4$ and graphite/graphite symmetric cells, as well as $LiMn_{0.6}Fe_{0.4}PO_4$/graphite pouch cells after formation at 3.90 V, obtained from equivalent circuit fitting at 10 ºC. The equivalent circuit can be referred to Figure S1.

Electrolytes	Pouch (Ω cm^2)	+/+ /2 (Ω cm^2)	-/- /2 (Ω cm^2)
CTRL	62.59	26.32	34.90
CTRL+2VC	96.54	27.52	54.75
CTRL+2VC1DTD	100.7	58.65	32.56

Table S10. Summary of R_{ct} values for $LiMn_{0.6}Fe_{0.4}PO_4$/$LiMn_{0.6}Fe_{0.4}PO_4$ and graphite/graphite symmetric cells, as well as $LiMn_{0.6}Fe_{0.4}PO_4$/graphite pouch cells after long-term cycling at 3.90 V, obtained from equivalent circuit fitting at 10 ºC. The equivalent circuit can be referred to Figure S1

Electrolytes	Pouch (Ω cm^2)	+/+ /2 (Ω cm^2)	-/- /2 (Ω cm^2)
CTRL	170.4	120.7	46.38
CTRL+2VC	186.3	131.2	64.13
CTRL+2VC1DTD	204.4	170.5	38.20

Table S11. Summary of increase rate of R_{ct} per cycle for $LiMn_{0.6}Fe_{0.4}PO_4$/$LiMn_{0.6}Fe_{0.4}PO_4$ and graphite/graphite symmetric cells, as well as $LiMn_{0.6}Fe_{0.4}PO_4$/graphite pouch cells.

Electrolytes	Pouch (Ω cm^2 $cycle^{-1}$)	+/+ /2 (Ω cm^2 $cycle^{-1}$)	-/- /2 (Ω cm^2 $cycle^{-1}$)
CTRL	0.6534	0.5720	0.0696
CTRL+2VC	0.2274	0.2625	0.02375
CTRL+2VC1DTD	0.1700	0.18336	0.0092

Table S12. Binding energies of peak assignment in the XPS spectra (**Figure S8**)

Peaks	Binding energy (eV)	Species
F 1s	689[6, 7]	C-F
	687[4, 8]	P-F
	685[4, 8]	LiF
O 1s	534.5[9, 10]	Oligo VC
	533-533.5[4, 9, 10]	C-O
	530.7[9, 10]	ROLi
C 1s	288[4, 11]	C=O/C-O=O
	286.7[4, 11]	C-O/C-O-C
	285[10, 11]	C-C/C-H
	283[9, 10]	LiC_6

Table S13. Energy information for the four different types of (010) lattice surfaces: Li-top, Mn/Fe-top, Li-O-top, and Mn/Fe-O-top

Surface type	Atom Movement Restriction	DFT Total Energy (eV)	Relative Energy (eV)
Li-top	1 layer at Bottom	-100460.217	73.486
Mn/Fe-top	1 layer at Bottom	-100533.685	0.000
Li-O-top	1 layer at Bottom	-100441.305	92.380
	2 layers at Bottom	-100456.313	77.371
Mn/Fe-O-top	1 layer at Bottom	-100518.895	14.790
	2 layers at Bottom	-100510.980	22.704

References

1. Levit, O.; Xu, P.; Shvartsev, B.; Avioz Cohen, G.; Stanciu, L.; Tsur, Y.; Ein-Eli, Y., Interphases Formation and Analysis at the Lithium–Aluminum–Titanium–Phosphate (LATP) and Lithium–Manganese Oxide Spinel (LMO) Interface during High-Temperature Bonding. *Energy Technology* **2020,** *8* (12), 2000634.
2. Jayakumar, R.; Pollard, T. P.; Borodin, O.; Shipitsyn, V.; Chak, C.; Pastel, G.; Zheng, A.; Johnson, M.; Hasan, F.; Bejger, C. M.; Schroeder, M. A.; Greenbaum, S. G.; Zuo, W.; Ma, L., Weakly solvating ester electrolyte for high voltage sodium-ion batteries. *Nano Energy* **2024,** *128*, 109969.
3. Keefe, A. S.; Buteau, S.; Hill, I. G.; Dahn, J. R., Temperature Dependent EIS Studies Separating Charge Transfer Impedance from Contact Impedance in Lithium-Ion Symmetric Cells. *Journal of The Electrochemical Society* **2019,** *166* (14), A3272.
4. Keefe, A. S.; Weber, R.; Hill, I. G.; Dahn, J. R., Studies of the SEI layers in Li(Ni0.5Mn0.3Co0.2)O2/Artificial Graphite Cells after Formation and after Cycling. *Journal of The Electrochemical Society* **2020,** *167* (12), 120507.
5. Chen, C. H.; Liu, J.; Amine, K., Symmetric cell approach and impedance spectroscopy of high power lithium-ion batteries. *Journal of Power Sources* **2001,** *96* (2), 321-328.
6. Wu, M.-S.; Zhang, X.-P.; Li, C.-Y.; Wang, Q.-Y.; Rong, Y.-J.; Liao, Y.-L.; Gao, M.-L.; Chen, W.-R., Stabilizing Lithium-Oxygen Batteries through In Situ Generated Phenyl/LiF-Rich Hybrid SEI Layer with Sulfonyl Fluoride Electrolyte Additive. *Journal of The Electrochemical Society* **2024,** *171* (2), 020554.
7. Zhang, S.; Li, W.-J.; Ling, S.-G.; Li, H.; Zhou, Z.-B.; Chen, L.-Q., Instability of lithium bis(fluorosulfonyl)imide (LiFSI)–potassium bis(fluorosulfonyl)imide (KFSI) system with LiCoO2 at high voltage*. *Chinese Physics B* **2015,** *24* (7), 078201.
8. Ma, X.; Young, R. S.; Ellis, L. D.; Ma, L.; Li, J.; Dahn, J. R., 1,2,6-Oxadithiane 2,2,6,6-tetraoxide as an Advanced Electrolyte Additive for Li[Ni0.5Mn0.3Co0.2]O2/Graphite Pouch Cells. *Journal of The Electrochemical Society* **2019,** *166* (12), A2665.
9. Madec, L.; Petibon, R.; Xia, J.; Sun, J. P.; Hill, I. G.; Dahn, J. R., Understanding the Role of Prop-1-ene-1,3-Sultone and Vinylene Carbonate in LiNi1/3Mn1/3Co1/3O2/Graphite Pouch Cells: Electrochemical, GC-MS and XPS Analysis. *Journal of The Electrochemical Society* **2015,** *162* (14), A2635.
10. Madec, L.; Xia, J.; Petibon, R.; Nelson, K. J.; Sun, J.-P.; Hill, I. G.; Dahn, J. R., Effect of Sulfate Electrolyte Additives on LiNi1/3Mn1/3Co1/3O2/Graphite Pouch Cell Lifetime: Correlation between XPS Surface Studies and Electrochemical Test Results. *The Journal of Physical Chemistry C* **2014,** *118* (51), 29608-29622.
11. Chen, X.; Wang, X.; Fang, D., A review on C1s XPS-spectra for some kinds of carbon materials. *Fullerenes, Nanotubes and Carbon Nanostructures* **2020,** *28* (12), 1048-1058.